Dimensional changes in highly oriented pyrolytic graphite due to electron-irradiation

Dimensional changes in highly oriented pyrolytic graphite due to electron-irradiation

J. Koike
Oregon State University, Corvallis, Oregon 97331-6001

D. F. Pedraza
Oak Ridge National Laboratory, P.O. Box 2003, Oak Ridge, Tennessee 37831-7274

(Received 29 November 1993; accepted 1 March 1994)

One of the main problems found in the nuclear applications of graphite is its dimensional instability under irradiation, involving both swelling and shape changes. In order to understand better the mechanisms that give rise to these changes, highly oriented pyrolytic graphite was irradiated with 300 keV electrons at temperatures between 25 and 657 °C in a transmission electron microscope (TEM). Microscopic dimensional changes and structural disordering were studied in directions parallel and perpendicular to the graphite basal plane. Changes in the specimen length were investigated by measuring the distance between two markers on the specimen surface in TEM images. Changes in the lattice parameter and the crystalline structure were studied by a TEM diffraction technique. In agreement with reported results, large increases in the specimen length and the lattice parameter were observed along the *c*-axis direction, whereas a relatively small decrease was observed along the *a*-axis. In irradiation studies conducted at room temperature, it was found that the dimensional change saturates at high dose, at an elongation along the *c*-axis direction of about 300%. High resolution microscopy revealed that the microstructure had become nanocrystalline. Electron energy loss spectroscopy results showed that the volume change was recovered at this stage. These observations are discussed in terms of point defect evolution and its effects on the microstructure of irradiated graphite.

I. INTRODUCTION

Graphite is a material of choice in nuclear applications, both fission and fusion, due to its extremely low neutron absorption cross section. However, it is well known that its thermal and mechanical properties are altered in an irradiation environment capable of producing displacement damage, whether the damaging particles are neutrons, electrons, or ions.[1–8] In such environments, not only do these physical properties become altered with increasing irradiation fluence, but also substantial dimensional changes take place that must be taken into account when designing nuclear components or using ion beams to modify the material's surface. Both dimensional and property changes are a result of displacement damage. The microstructure that evolves depends on damage rate, irradiation temperature, and damaging particle. At temperatures of normal operation in a reactor or those employed for ion implantation, the developing microstructure is substantially different from the initial one. In general, the residual damage is a matter of kinetics in which damage creation and annealing are competing mechanisms of defect evolution. Thus, it can be expected that residual damage at a given temperature and fluence will decrease as the displacement rate is decreased, provided point defects are significantly mobile. Increasing temperatures allow faster annealing of damage by retarding, or even preventing at fairly high temperatures, microstructural changes.

Microstructural evolution has been previously studied by transmission electron microscopy (TEM) of ion implanted,[1] ion irradiated,[2] neutron irradiated,[3] and electron irradiated graphite.[4–8] For room temperature irradiations with any one of the particle types, high resolution electron microscopy (HREM) reveals a similar pattern of graphite structure and evolution, a progressive disorder with increasing dose. Selected area diffraction observations and electron energy loss spectroscopy (EELS) of electron irradiated highly oriented pyrolytic graphite (HOPG) are consistent with the HREM results.[7,8] Although crystalline order was found to persist along the *c*-axis up to a dose of ~1 dpa (displacement per atom) for 300 keV electrons and, for instance, to fluences on the order of 1×10^{14} Sb-ions/cm^2 at 30 keV,[9] loss of long range order was initiated in the basal planes as manifested by the breakup of lattice fringes, observed by HREM, into small segments 0.5 to 5 nm in length. Rotation of these small segments by a small angle, ~15° relative to the original (0001) planes, was the signature of the initial irradiation-induced disordering process and was interpreted as an actual fragmentation of the

basal planes.[7,8] In ion-irradiated graphite, swelling has been detected[10,11] accompanied by anisotropic dimensional changes, similar to those occurring under neutron irradiation.[12] Also, increasing ion damage revealed a complete loss of crystalline order in three dimensions at a dose of 1×10^{15} Sb-ions/cm^2 at 30 keV, whose HREM image showed no lattice fringes, but rather a texture resembling that of amorphous carbon.[4,9] Although amorphous carbon undergoes structural changes under ion irradiation, as revealed by Raman spectroscopy,[13,14] no measurements exist as to whether it also undergoes dimensional changes. Concerning neutron irradiation, on the other hand, there is no proof that prolonged irradiations lead to an amorphous structure.[15] However, measurements in pyrolytic graphites demonstrate persistence of dimensional changes to fairly high doses, on the order of tens of dpa's.[10]

In terms of dose rates (dpa/s: displacement per atom per second), electron irradiation is similar to ion irradiation rather than to common neutron irradiation (on the order of 1×10^{-4} to 1×10^{-3} dpa/s vs 1×10^{-7} dpa/s for neutrons). However, ion irradiation results in point defect clustering due to an initial spacial distribution of damage in a displacement cascade in contrast to isolated point defects produced by electron bombardment. On the other hand, the low dose rate employed for neutron irradiation may favor recombination events resulting in less clustering. It can thus be asked whether irradiation effects produced by either class of irradiation have common aspects with electron-irradiation generated effects, and whether the latter can be used to interpret irradiation effects under neutron or under ion irradiation. Aiming at answering these questions, we have investigated the changes in dimensions, lattice parameters, and microstructure in HOPG produced by electron irradiation in the temperature range from ~25 °C and 657 °C.

II. EXPERIMENTAL PROCEDURE

Highly oriented pyrolytic graphite was sliced across the basal plane orientation to a thickness of ~1 mm, using a slow speed diamond saw. The slice was mechanically ground on one side with a final grid size of 3 μm and mounted with epoxy on a slotted copper grid with the ground side facing the copper grid. The other side was further ground and dimpled to a thickness of less than 30 μm. The specimen was then ion-milled to electron transparency at room temperature, using 5 keV Ar-ions until a perforation was formed. The specimen prepared in this way has the graphite basal plane perpendicular to the copper grid plane. Thus, the crystallographic *c*-axis lies on the grid plane. The specimen was mounted on a double-tilt heating stage for irradiation inside a TEM at elevated temperatures. A foil with its surface normal to the basal planes was prepared by slicing a thin slab across the basal plane from HOPG. The thin slab was next mounted on a slotted Cu grid, mechanically ground, and ion milled to perforation.

An accelerating voltage of 300 kV was employed for TEM. For normal operation such as in diffraction or bright-field mode, the electron beam was spread to minimize irradiation damage to the specimen during observation time. For irradiation purposes, the electron beam was focused to a diameter of approximately 0.6 μm. The flux was 6×10^{19} e/cm^2-s, producing a displacement dose rate of 5.2×10^{-4} dpa/s.[7] Because of the good thermal conductivity and the structural integrity of HOPG, beam heating is relatively small (an estimated value of 10 °C).

The specimen was irradiated at temperatures of 25, 146, 280, 420, and 657 °C. The dimensional changes were studied by measuring the distance between conspicuous markers such as specimen edges and contamination spots. Contamination spots are produced by focusing the electron beam while heating the specimen at high temperature for a short period of time. Structural changes were observed by HREM. Lattice parameter variations were obtained by measuring the distance of crystalline spots in selected area diffraction patterns. Care was taken to properly orient the specimen so as to satisfy a Bragg diffraction condition accurately by strongly exciting a desired diffraction spot. A room temperature irradiated specimen was annealed stepwise up to 657 °C *in situ* in the electron microscope in order to test the stability of the irradiation-induced structural changes. Electron energy loss spectroscopy was also employed to obtain information on the density change of irradiated HOPG through the plasmon peak shift.

III. RESULTS

A. Dimensional changes

The morphology of the specimen before irradiation can be seen in Fig. 1(a). The banded morphology in the bright-field (BF) image is interrupted by breaks along the basal planes, the upper edge borders with the perforation produced during ion milling. These elongated pores are most likely a result of specimen preparation rather than a growth defect, and occur because of the weak binding forces that exist between basal planes. The *c*-crystallographic axis is perpendicular to the line of the breaks, lying on the plane of the figure. Morphological changes occurring with increasing electron fluence during irradiation at room temperature can be seen in Figs. 1(b) and 1(c). Elongation along the *c*-axis is clearly noticeable, as well as progressive contraction along basal plane directions as the dose is increased to 0.50 dpa [Fig. 1(b)] and 1.40 dpa [Fig. 1(c)].

The dimensional changes were quantitatively studied by irradiating a strip of graphite attached to the rest of

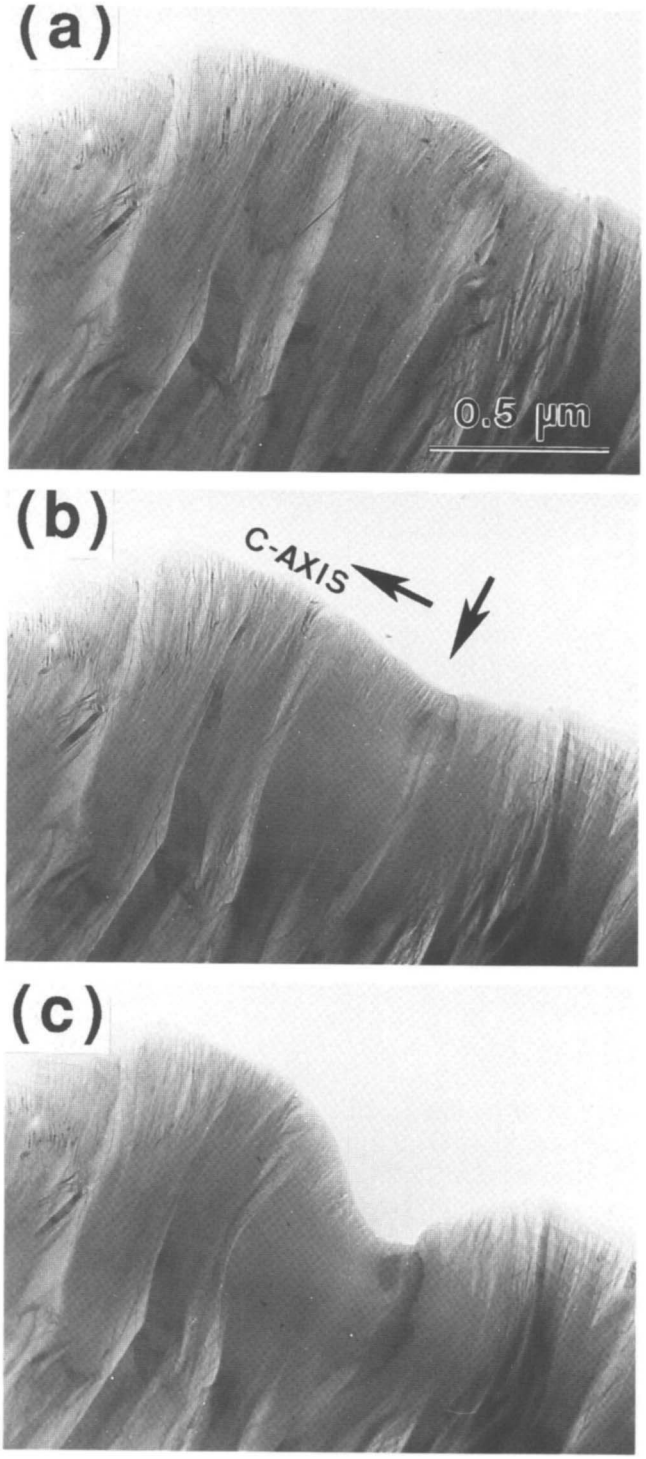

FIG. 1. Bright-field images of HOPG specimen with the c-crystallographic axis normal to the electron beam, before irradiation (a) and after 300 kV electron irradiation to 0.50 dpa (b) and 1.4 dpa (c). The irradiated region, indicated with an arrow parallel to the basal plane, is easily visible at the center of the micrographs. Notice the strong expansion along the c-axis direction and the contraction normal to it on the plane of the micrograph.

the specimen by one end only. In this way, the specimen can alter its shape and size with very little restraint from the surrounding unirradiated crystal. Results for room temperature irradiations are shown in Figs. 2 and 3. Figure 2 shows the morphological variations in BF images, where the basal plane is parallel to the electron beam incidence. The irradiated area is circled with a dotted line, indicating the size of the electron beam. It can also be noticed, looking at the image of the unirradiated specimen, that the beam diameter is larger than the width of the strip. After irradiation to 1.35 dpa, considerable elongation along the c-axis occurred and the entire beam was thereafter fully incident onto a specimen area. Further irradiation to a dose of 5.0 dpa gave rise to continuous elongation by 290% of the initial width of the graphite strip. The irradiation-induced strain along the c-axis as a function of dose is plotted in Fig. 3. It was obtained from the measured distance change between the edges farthest apart in the c-axis divided by the initial strip width. As seen in this figure, the elongation rate is initially fast up to a dose of ~0.2 dpa. A slower strain increase follows at a constant rate up to 4.0 dpa. Beyond the latter dose, the swelling rate shows saturation at a strain level of approximately 300% at 6 dpa. However, this is not the true saturation value, since above 1.35 dpa the beam was no longer incident on the entire area being measured. A larger saturation value would have been obtained if a larger beam was employed to ensure that the entire area was irradiated.

The dimensional change along the c-axis, $\Delta l_c/l_{co}$, was studied at elevated temperatures, and the results are shown in Fig. 4(a). Δl_c is the change in height of the strip, as seen in Fig. 1, and l_{co} is the original height. At all examined temperatures, progressive elongation was observed with increasing electron dose. With increasing temperature, on the other hand, the elongation rate decreases. Notice that at a temperature between 420 and 657 °C this trend apparently reverts. This reversion has also been observed upon neutron irradiation of graphite above 600 °C.[7] The dimensional change along the basal plane was also measured, using markers of contamination spots made outside the irradiated area. The plotted value, $\Delta l_a/l_{ao}$, was calculated as the ratio of the change in distance between the contamination spots, Δl_a, over the electron beam diameter, l_{ao}. The results obtained at 146, 280, and 420 °C are shown in Fig. 4(b). However, these values are lower than the actual strain along the basal plane because the region being irradiated is always augmented. Nonetheless, the strain along basal plane directions is always compressive, contrary to the strain along the c-axis direction. The negative value always increases with dose and decreasing irradiation temperature in the measured ranges.

The volume change cannot be calculated from the values given in Figs. 4(a) and 4(b) not only because the actual strain along the basal plane is less than the values plotted in Fig. 4(b), but also because the beam

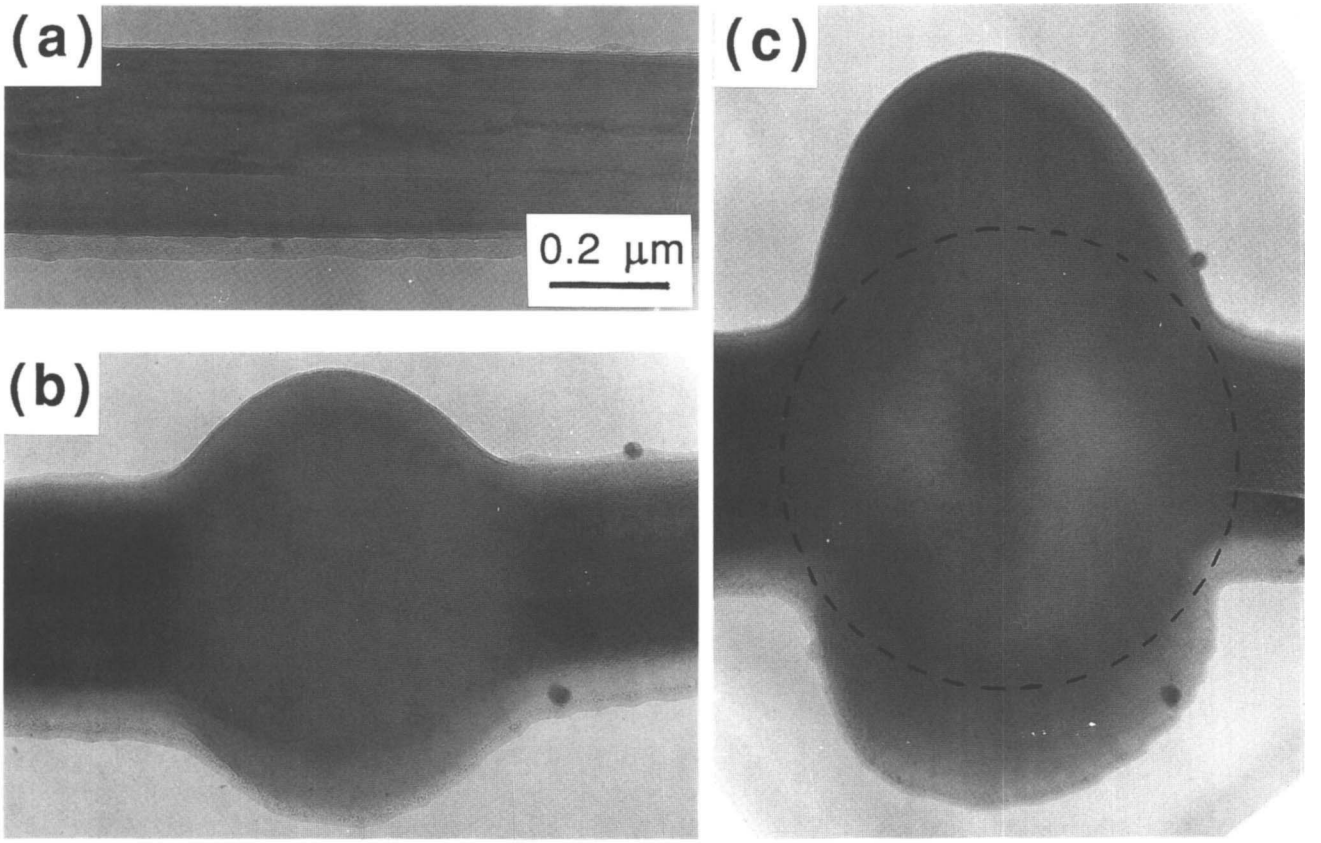

FIG. 2. Bright-field images of an HOPG strip illustrating the radical morphological changes produced by 300 keV electron irradiation at room temperature: (a) before irradiation, (b) after irradiation to 1.35 dpa, and (c) after irradiation to 5.0 dpa. The dotted circle indicates the size of the incident beam.

intensity is not uniform. In order to calculate the volume change within the present experimental conditions, we have used a different TEM technique, electron energy loss spectroscopy (EELS), which allows one to probe a central area exposed to irradiation throughout one experiment.

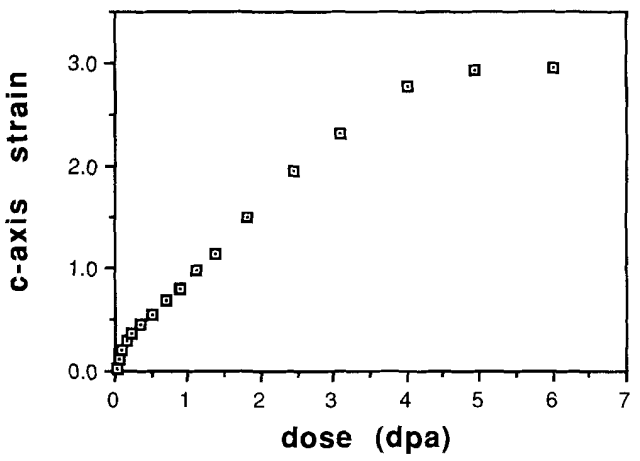

FIG. 3. Room temperature irradiation-induced strain along the *c*-axis as a function of dose showing saturation after a dose of ~4 dpa.

B. Structural evolution

Structural changes caused by irradiation were studied by examining selected area diffraction (SAD) patterns after irradiation to a dose of 1 dpa. When the specimen was irradiated along the $[1\bar{2}10]$ direction, strong diffuse intensities concentrated around the 0002 spot of crystalline graphite, as seen in Fig. 5, indicating the retention of crystalline order along the *c*-axis. By contrast, when the specimen was irradiated along the [0001] direction, a continuous diffuse ring was observed as shown in Fig. 6(a). The radius of the first ring is close to the distance of the $1\bar{1}00$ spot of the crystal structure. The occurrence of the diffuse ring in the diffraction pattern is generally interpreted as a characteristic of an amorphous structure. However, when this specimen was tilted in an arbitrary direction by 46°, an asymmetric intensity was revealed inside the first ring, as shown in Fig. 6(b). Therefore, independent of irradiation direction, the periodicity along the *c*-axis is retained at least up to a dose of 1 dpa. But, as the diffuse ring suggests, the long range periodicity in the basal plane appears to be lost by irradiation to this dose.

A specimen irradiated at room temperature to a dose of 1.3 dpa was later annealed in the TEM starting at

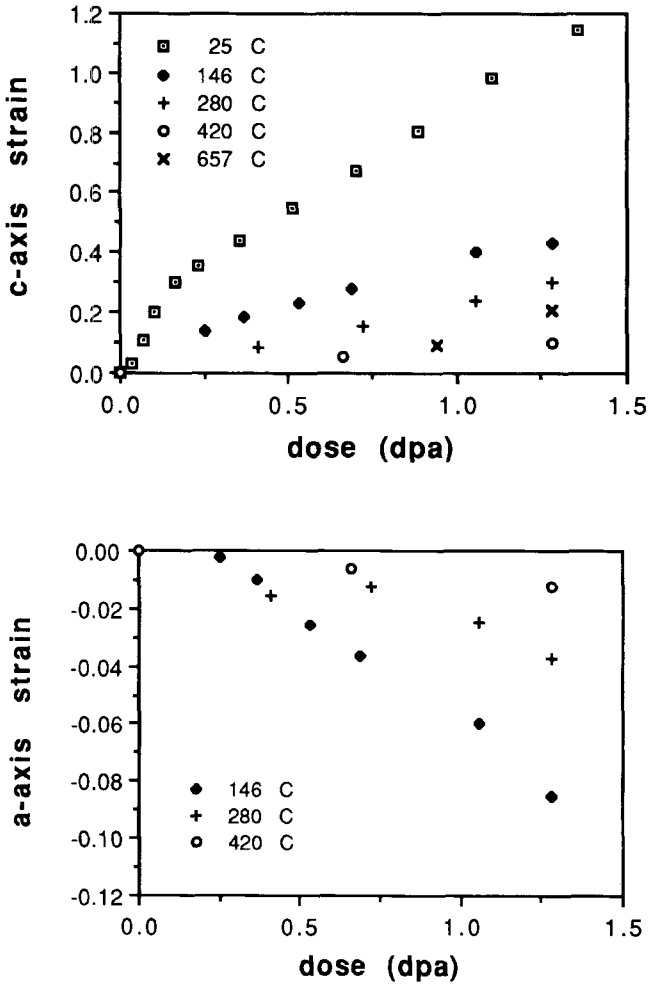

FIG. 4. Dimensional changes induced by irradiation at various temperatures.

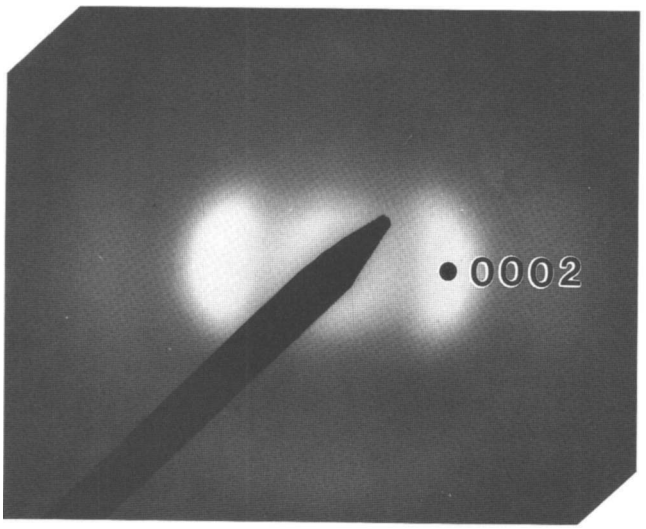

FIG. 5. Selected area diffraction pattern after irradiation to a dose of 1 dpa. Electron beam was parallel to the [1$\bar{2}$10] direction.

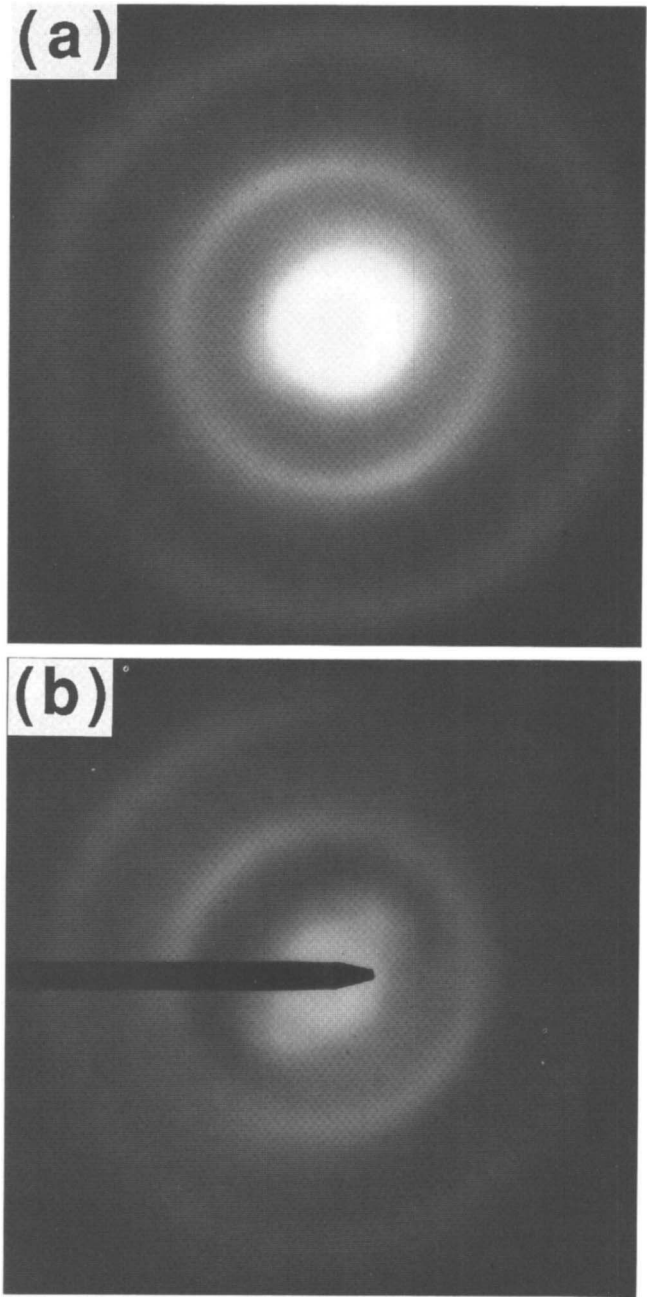

FIG. 6. Selected area diffraction patterns after irradiation to a dose of 1 dpa: (a) electron beam parallel to foil normal ([0001] direction), and (b) foil normal tilted 46° relative to the electron beam.

63 °C. The temperature was increased stepwise by 20 or 30 °C, holding the specimen for about 300 s at each step, and for 1 h at the highest reached temperature of 657 °C. A comparison of the SAD pattern of the annealed specimen shown in Fig. 7 with the pattern shown in Fig. 5 reveals sharpening of the arc intensities after annealing, indicating some recovery of the graphite structure. However, the spread of basal plane orientations remains, as indicated by the intensity distribution along

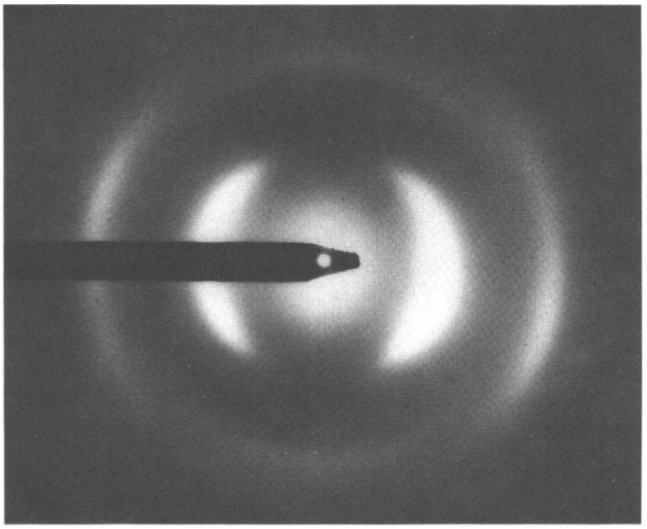

FIG. 7. Selected area diffraction patterns after irradiation to a dose of 1.3 dpa and subsequent *in situ* annealing up to 1 h at 657 °C. Electron beam was parallel to foil normal ([0001] direction).

a wide arc around the 0002 spot. The first indication of this recovery was in fact noticed after the 450 °C anneal.

In order to understand the origin of swelling, the atom-level structure and lattice parameter changes were studied in further detail during room temperature irradiation. The results of lattice parameter change are plotted in Fig. 8 as fractional changes relative to an initial value of lattice parameter determined by the position of the 0002 and the $1\bar{1}00$ spots. The lattice parameter along the *c*-axis direction is found to increase rapidly with increasing dose and appears to attain a constant value 4% larger at a dose larger than 0.05 dpa to 0.06 dpa. At higher doses, the diffraction spot becomes too broad to determine its position with reasonable accuracy. Along the basal plane, the lattice parameter decreases with increasing dose rapidly up to a dose of 0.03 dpa, then

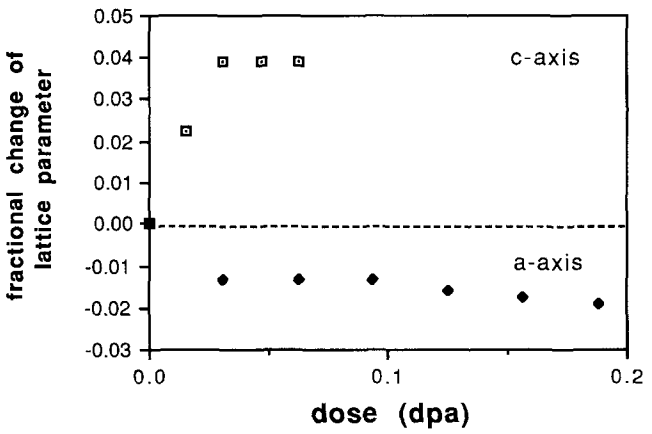

FIG. 8. Fractional changes of lattice parameters induced by irradiation at room temperature, as a function of dose.

it decreases more gradually at higher doses. The crystalline spot remains sufficiently sharp to calculate lattice parameter up to a dose of 0.18 dpa at which the lattice parameter has decreased by nearly 2%.

The variation of the atom-level structure during irradiation is shown in Fig. 9. The basal planes, oriented parallel to the incident electron beam direction, are seen edge-on before irradiation in Fig. 9(a). After irradiation to 1 dpa, the lattice fringes of the basal planes are broken up into small segments of 0.5 to 5 nm in length tilted with respect to each other by an angle of approximately 15°. However, it is still easy to identify the persistence of crystalline order along the *c*-axis in the image. After irradiation to 6 dpa, the high resolution image taken from the central part of the irradiated area shows no trace of the original crystalline periodicity. Instead, the structure can be described as randomly oriented nanocrystals characterized by many well-defined sets of lattice fringes observed on a nanometer scale.

C. Electron energy loss spectroscopy

The density change during electron irradiation was deduced from the plasmon peak shift in the electron energy loss spectra. It was assumed that the number of valence electrons per atom remained constant during the structural evolution occurring during irradiation. The energy loss spectra acquired from the unirradiated specimen and after irradiation to 1 dpa and to 6 dpa are respectively shown in Figs. 10(a)–10(c). The plasmon peak position was determined by fitting the experimental curves by a Lorentzian function. As already reported,[7,8] irradiation to a dose of 1 dpa produces a density drop of 8.9%. However, after the higher dose of 6 dpa the initial density is recovered.

IV. DISCUSSION

Under electron irradiation, the structure along the basal plane becomes disordered and is associated with fragmentation. We have previously suggested a fragmentation mechanism based on the interaction between vacancies and interstitial clusters.[8] It has been reported that vacancies in graphite are immobile up to ~900 °C.[16] On the other hand, interstitials are mobile well below ambient temperature and may form planar clusters consisting of 4 ± 2 atoms at temperatures lower than 300 °C.[17] No interstitial loops were observed at these low temperatures in electron-irradiated HOPG. In our proposed mechanism, these small interstitial clusters fracture the lattice at "soft" spots such as those where the lattice has relaxed around vacancies. Computer modeling of this mechanism allowed us to gain further understanding on the force driving the fracture of the basal plane.[18] We have shown that the tendency to recombination of an interstitial and a vacancy remains very strong, even if the

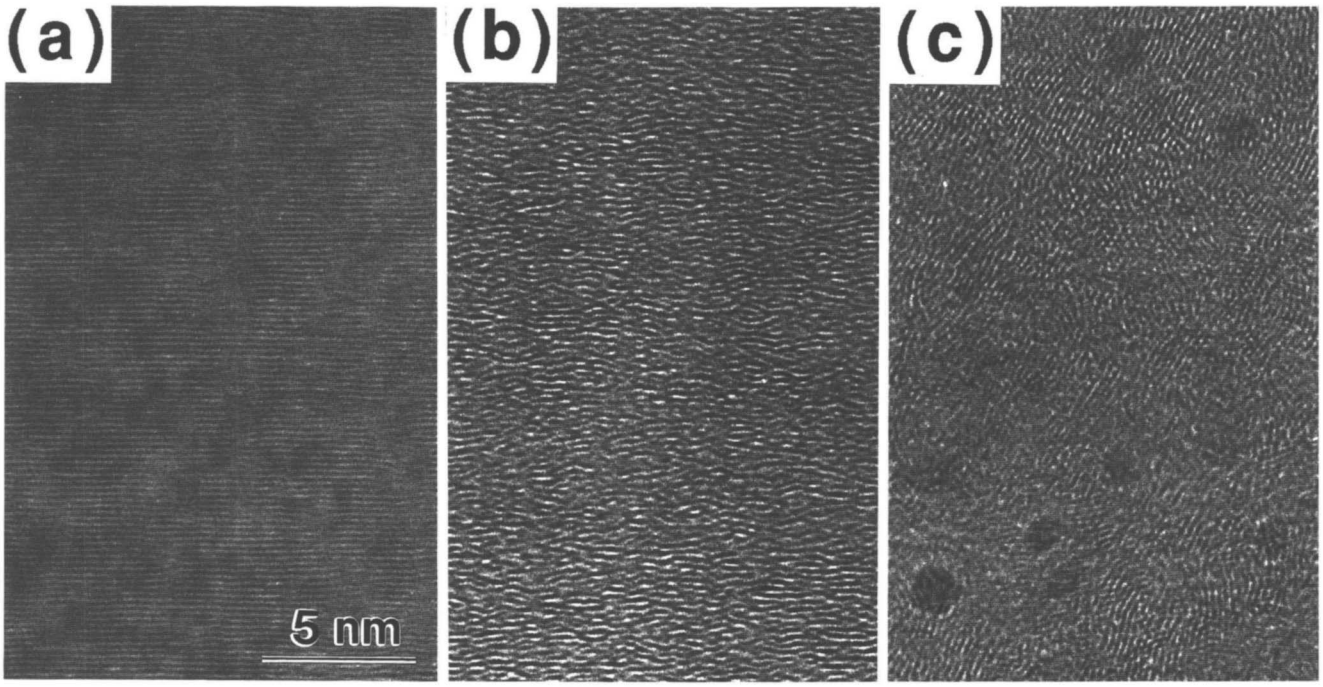

FIG. 9. High resolution lattice fringe images of HOPG: (a) before irradiation, (b) after a dose of 1 dpa, and (c) after a dose of 6 dpa.

interstitial belongs to a cluster. Because the interstitial does not sever its bonding with the other atoms in the cluster, the force driving to recombination destabilizes the relaxed bonds around the vacancy, producing the fracture and the tilting of the resulting fragment. This means that atomic bonding with the cluster should be more rigid than the relaxed bonding around the vacancy. Upon recombination of a clustered interstitial with a vacancy, fracture is initiated at the "soft" spot in the basal plane where the lattice has relaxed around the vacancy. As the dose is increased and more locations in the basal plane are fractured, it is likely that damage production and recovery are balanced and that fragments interact to form a nanocrystalline structure. It should be noted that the final structure depends on kinetic restrictions and is controlled by a dynamical balance between damage production and recovery. If damage production rate is much faster than that employed in the present experiment, the fragment size is expected to become smaller and may lead eventually to amorphization.

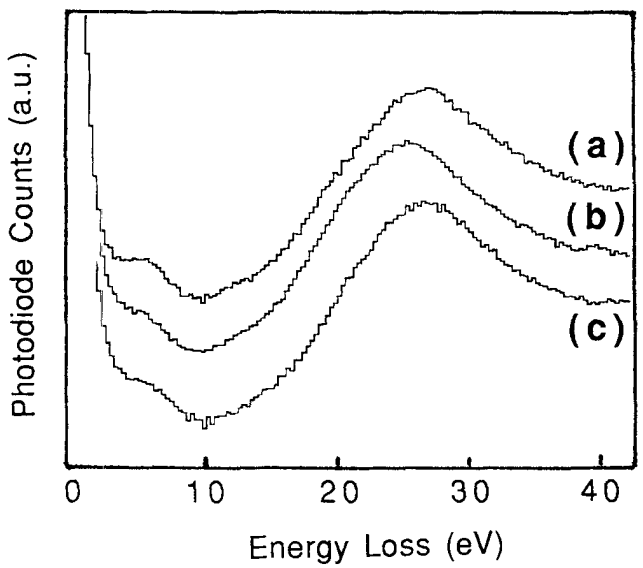

FIG. 10. Electron energy loss spectra showing zero-loss plasmon peaks: (a) before irradiation, (b) after a dose of 1 dpa, and (c) after a dose of 6 dpa.

In fact, low dose ion irradiation at room temperature appears to produce a damage structure entirely similar to the damage induced by electrons. However, at higher doses the formation of an amorphous structure has been reported under room temperature ion irradiation, e.g., 30 keV Sb or 30 keV Bi to doses of 1×10^{15} ions/cm^2 (Ref. 9) as well as 35 keV C ion irradiation to 1×10^{16} ions/cm^2.[19] Such a difference between the irradiated structure produced by electrons and by ions has been reported in many materials, and it is due to the different damage structure caused by each particle type: point defect formation by electrons versus displacement cascade damage by heavy ions. Similar to ions, neutrons are considered to form displacement cascade damage. However, the structure observed by HREM[3] appears to be rather similar to that irradiated by electrons. As discussed in Ref. 20, displacement cascades in graphite are not as dense as in other close-

packed materials because of the large space existing between the basal planes which is much higher than the screening radius of the carbon ion core.[21] Considering that neutron dose rates commonly existing in a reactor environment are substantially lower than those employed in ion irradiation, this low density of displaced atoms in a cascade damage may be easily annealed out, leaving a small number of point defects before another cascade is formed.[20] Therefore, it is very likely that there are similarities between neutron and electron irradiations. If a continuous neutron dose rate comparable to that of ion irradiation could be used, neutron damage might be expected to be similar to ion damage. On the other hand, as the irradiation temperature is raised, recombination can become prevalent also under ion irradiation due to increased interstitial mobility which combined with a high rate of defect production results in a high recombination rate. A remarkable decrease of irradiation damage is certainly observed by Raman spectroscopy on ion implantation at a temperature as low as 300 °C.[10,14]

The annealing experiment indicated a recovery of radiation damage produced by room temperature irradiation. The distinct recovery was observed in the diffraction pattern above 450 °C. Although it was not detected by the diffraction technique, damage recovery might even have started at a lower temperature. Differential scanning calorimetry has shown the onset of heat release in neutron-irradiated graphite at 150 °C.[22] As seen in the temperature-dependent *c*-axis elongation, the magnitude of the elongation decreases progressively with increasing irradiation temperature caused by increasing damage annealing. However, the magnitude of the elongation was observed to increase slightly when the irradiation temperature was increased from 420 to 657 °C. A similar reversal trend has been observed in neutron-irradiated graphite. The onset of a new damage annealing process seems to occur between 420 and 657 °C and could lead to a different pattern of microstructural evolution, but the exact process is not known at the present time. This change in behavior suggests that the irradiation-induced growth mechanisms at higher temperatures may be quite different from those occurring at temperatures lower than ~600 °C, and, hence, whether or not saturation occurs is an open question.

High dose (5 dpa) room temperature electron irradiation of graphite showed a significant dimensional change higher than reported under neutron irradiation at 450 °C (a *c*-axis elongation of 200% after 70 dpa). Following the results of neutron irradiation, it seemed as though irradiation growth could proceed almost indefinitely. However, in the present study we have demonstrated that the dimensional change under 300 keV electron irradiation at room temperature can saturate at a *c*-axis elongation of $\Delta l_c/l_{co} > 300\%$. It might be argued that the proximity of free surfaces plays an important role in the attainment of damage saturation in the present experiments. This argument is, however, countered by the fact that saturation appears to be consistent with the evolution of the HREM microstructure. The present results clearly indicated a continuous transition from the anisotropic to the isotropic structure with increasing electron dose. The transition takes place by the fragmentation of basal planes and concomitant tilting of these fragments, and finally the formation of a stable nanocrystalline structure. As the crystallinity is recovered on a localized scale by forming nanocrystals, the local density may also increase. This may be the explanation for the density recovery calculated from the plasmon peak shift during irradiation from 1 dpa to 5 dpa. On the other hand, disordering along and near the nanograin boundaries is expected to give rise to a plasmon peak at a lower energy position in addition to the one at the original position. However, the EELS spectrum of the specimen irradiated to 5 dpa did not show any notable peak at a lower energy. In order to derive an accurate structural model consistent with both the HREM and EELS results, more work is needed, particularly quantitative evaluation of the crystalline perfection within the nanograins and the effects of disordered boundary regions on the plasmon peak position.

The present results demonstrate that low dose irradiation damage is not sufficient to predict microstructural changes at higher doses. They also suggest that neutron irradiation under reactor conditions, where the dose rate is low, may be better simulated by electron than by ion irradiation. A comparison of dimensional changes is not straightforward. Due to the low defect production rate under neutrons, a higher temperature is required for effective clustering to take place. However, because recombination is also enhanced, the total dose to produce equivalent effects should be higher. This point is well illustrated with the example mentioned earlier of a dimensional change produced by room temperature electron irradiation to a dose of 5 dpa somewhat larger than that produced by neutron irradiation at 450 °C to a dose of 70 dpa. Whereas the electron damage was already saturated, this was still not the case with the neutron damage.

ACKNOWLEDGMENTS

This research was sponsored by the Office of Fusion Energy, United States Department of Energy, under Contract DE-AC05-84OR21400 with Martin Marietta Energy Systems, Inc. The use of the SHaRE electron microscopy facility at ORNL is gratefully acknowledged.

REFERENCES

1. L. Salamanca-Riba, G. Braunstein, M. S. Dresselhaus, J. M. Gibson, and M. Endo, Nucl. Instrum. Methods, Phys. Res. B **7/8**, 487 (1985).

2. H. Shimizu, S. Suginuma, and Y. Gotoh, J. Nucl. Mater. **176–177**, 1000 (1990).
3. T. Tanabe, S. Muto, Y. Gotoh, and K. Niwase, J. Nucl. Mater. **175**, 258 (1990).
4. Y. Gotoh, H. Shimizu, and H. Murakami, J. Nucl. Mater. **162–164**, 851 (1989).
5. A. Matsunaga, C. Kinoshita, K. Nakai, and Y. Tomokiyo, J. Nucl. Mater. **179–181**, 457 (1991).
6. T. Tanabe, S. Muto, and K. Niwase, Appl. Phys. Lett. **61**, 1638 (1992).
7. J. Koike and D. F. Pedraza, in *Beam-Solid Interactions: Fundamentals and Applications*, edited by M. A. Nastasi, L. Harriot, N. Herbots, and R. S. Averback (Mater. Res. Soc. Symp. Proc. **279**, Pittsburgh, PA, 1993), p. 67.
8. J. Koike and D. F. Pedraza, in *International Conf. on Beam Processing of Advanced Materials*, edited by J. Singh and S. M. Copley (The Minerals, Metals and Materials Society, Warrendale, PA, 1993), p. 519.
9. M. Endo, L. Salamanca-Riba, G. Dresselhaus, and J. M. Gibson, J. Chimie Phys. **81**, 803 (1984).
10. M. S. Dresselhaus and R. Kalish, *Ion Implantation in Diamond, Graphite and Related Materials* (Springer-Verlag, Berlin, Germany, 1992).
11. B. K. Annis, D. F. Pedraza, and S. P. Withrow, J. Mater. Res. **8**, 2587 (1993).
12. B. T. Kelly, *Physics of Graphite* (Applied Science Publishers, London and New Jersey, 1981).
13. B. S. Elman, M. S. Dresselhaus, G. Dresselhaus, E. W. Maby, and H. Mazurek, Phys. Rev. B **24**, 1027 (1981).
14. D. Hembree, Jr., D. F. Pedraza, G. Romanoski, S. P. Withrow, and B. K. Annis, in *Beam-Solid Interactions: Fundamentals and Applications*, edited by M. A. Nastasi, L. Harriot, N. Herbots, and R. S. Averback (Mater. Res. Soc. Symp. Proc. **279**, Pittsburgh, PA, 1993), p. 15.
15. B. T. Kelly, J. Nucl. Mater. **172**, 237 (1990).
16. P. A. Thrower and R. M. Mayer, Phys. Status Solidi A **47**, 11 (1978).
17. D. G. Martin and R. W. Henson, Philos. Mag. **9**, 659 (1964).
18. D. F. Pedraza and J. A. Rifkin, unpublished.
19. E. A. Kenik, D. F. Pedraza, and S. P. Withrow, *Proceedings of the 51st Annual Meeting of the Microscopy Society of America* (1993), p. 1106.
20. D. F. Pedraza, in *Phase Formation and Modification by Beam-Solid Interactions*, edited by G. S. Was, L. E. Rehn, and D. M. Follstaedt (Mater. Res. Soc. Symp. Proc. **235**, Pittsburgh, PA, 1992), p. 437.
21. J. H. W. Simmons, *Radiation Damage in Graphite* (Pergamon Press, Oxford, 1965).
22. J. C. Bell, H. Bridge, A. H. Cottrell, G. B. Greenough, W. N. Reynolds, and J. H. W. Simmons, Philos. Trans. Roy. Soc. **A254**, 361 (1962).